Structural distortion below the Néel temperature in spinel GeCo_{2}O_{4}

Phillip T. Barton, Moureen C. Kemei, Michael W. Gaultois, Stephanie L. Moffitt, Lucy E. Darago, Ram Seshadri, Matthew R. Suchomel, and Brent C. Melot

Phys. Rev. B **90**, 064105 — Published 8 August 2014

DOI: 10.1103/PhysRevB.90.064105

Structural distortion below the Néel temperature in spinel $GeCo_2O_4$

Phillip T. Barton, Moureen C. Kemei,* Michael W. Gaultois,
Stephanie L. Moffitt, Lucy E. Darago, and Ram Seshadri†
Materials Department and Materials Research Laboratory,
University of California, Santa Barbara, CA, 93106, USA

Matthew R. Suchomel
X-Ray Science Division, Argonne National Laboratory, Argonne, IL 60439, USA

Brent C. Melot
Department of Chemistry, University of Southern California, Los Angeles, CA, USA

A structural phase transition from cubic $Fd\bar{3}m$ to tetragonal $I4_1/amd$ symmetry with $c/a > 1$ is observed at $T_S = 16\,K$ in spinel $GeCo_2O_4$ below the Néel temperature $T_N = 21\,K$. Structural and magnetic ordering appear to be decoupled with the structural distortion occurring at 16 K while magnetic order occurs at 21 K as determined by magnetic susceptibility and heat capacity measurements. An elongation of CoO_6 octahedra is observed in the tetragonal phase of $GeCo_2O_4$. We present the complete crystallographic description of $GeCo_2O_4$ in the tetragonal $I4_1/amd$ space group and discuss the possible origin of this distortion in the context of known structural transitions in magnetic spinels. $GeCo_2O_4$ exhibits magnetodielectric coupling below T_N. The related spinels $GeFe_2O_4$ and $GeNi_2O_4$ have also been examined for comparison. Structural transitions were not detected in either compound down to $T \approx 8\,K$. Magnetometry experiments reveal in $GeFe_2O_4$ a second antiferromagnetic transition, with $T_{N1} = 7.9\,K$ and $T_{N2} = 6.2\,K$, that was previously unknown, and that bear a similarity to the magnetism of $GeNi_2O_4$.

PACS numbers: 61.50.Ks, 75.50.Ee, 75.47.Lx

I. INTRODUCTION

The spinel crystal structure is of wide interest in condensed matter physics for diverse phenomena including heavy fermions,[1] multiferroic behavior,[2] and exotic states arising from geometric frustration.[3–5] The rich physics of complex transition metal oxides derives from the intricate interplay of charge, orbital, spin, and lattice degrees of freedom. In this report, we examine the magnetic and structural properties of the spinel $GeCo_2O_4$ that are largely influenced by competing orbital and spin degrees of freedom. We also study the structure and magnetism of the related systems GeM_2O_4 (M = Fe and Ni).

At room temperature, GeM_2O_4 (M = Fe, Co, and Ni) are cubic spinel oxides in the space group $Fd\bar{3}m$. Ge^{4+} cations are tetrahedrally coordinated by O^{2-} while M^{2+} cations occupy octahedral sites. The structures and magnetic behavior of all three GeM_2O_4 spinels were originally reported by Blasse and Fast in 1963.[6,7] $GeFe_2O_4$ is orbitally degenerate due to partially filled t_{2g}^4 states of octahedral high spin Fe^{2+}. $GeCo_2O_4$ has been the subject of many investigations because it has the unique electronic ground state of octahedral Co(II), which is high-spin $3d^7$, with $S = 3/2$ $L = 3$, though it is better described as a Kramer's doublet with $J_{\text{eff}} = 1/2$. The orbitally degenerate t_{2g}^5 states of high spin octahedral Co^{2+} give rise to spin-orbit coupling that results in a large single-ion anisotropy for a $3d$ transition metal. In contrast to $GeCo_2O_4$ and $GeFe_2O_4$, $GeNi_2O_4$ has a non-degenerate electronic ground state with fully occupied t_{2g}^6 levels and half occupied e_g^2 states of octahedral Ni^{2+}.

$GeCo_2O_4$, $GeFe_2O_4$, and $GeNi_2O_4$ exhibit antiferromagnetic order at temperatures below 30 K. $GeCo_2O_4$ has a Néel temperature near 21 K while $GeNi_2O_4$ shows two magnetic ordering anomalies at $\approx 12\,K$ and 11 K.[8–10] Our magnetic susceptibility studies of the spinel $GeFe_2O_4$ show that it also exhibits two antiferromagnetic transitions at 7.9 K and 6.2 K. The magnetic structure of the Ni and Co compounds consists of ferromagnetic (111) planes that are antiferromagnetically coupled with a $(\frac{1}{2}\ \frac{1}{2}\ \frac{1}{2})$ magnetic propagation vector.[9] In between the Kagome planes are triangular planes of spins whose orientation is not well known. Neutron diffraction measurements by Diaz *et al.* show that the triangular plane moments of $GeNi_2O_4$ are aligned parallel to the (111) direction while in $GeCo_2O_4$ the triangular plane moments are perpendicular to the (111) direction.[9] Diaz *et al.* have also shown that $GeCo_2O_4$ and $GeNi_2O_4$ systems undergo two subtle field-induced transitions above 4 T.[9]

Here, we study the low temperature tetragonal structural distortion of the spinel $GeCo_2O_4$. We find that the structural distortion is decoupled from antiferromagnetic ordering, occurring at $T_D = 16\,K$ rather than at the Néel temperature of 21 K. We resolve the low-temperature nuclear structure of $GeCo_2O_4$ by Rietveld refinement of high resolution synchrotron x-ray diffraction data using a tetragonal $I4_1/amd$ model with $c/a > 1$. The evolution of structure shows an elongation of CoO_6 octahedra in the tetragonal phase of $GeCo_2O_4$. We discuss the mechanisms behind the structural distortion of $GeCo_2O_4$ in the context of known structural distortions in magnetic

spinels. Synchrotron diffraction studies of $GeFe_2O_4$ and $GeNi_2O_4$ down to $\approx 8\,K$ show the absence of structural distortions in these systems above this temperature. We also report magnetodielectric coupling in $GeCo_2O_4$ beneath $T_N = 23\,K$, while $GeNi_2O_4$ shows no evidence for such behavior. Magnetic susceptibility studies of the related spinel, $GeFe_2O_4$, reveals two antiferromagnetic ordering temperatures of 6.2 K and 7.9 K.

II. METHODS

Polycrystalline GeM_2O_4 (M = Fe, Co, Ni) were prepared by solid-state reaction of powder reagents. Stoichiometric amounts of GeO_2 and either Fe/Fe_2O_3, Co_3O_4, or NiO were ground with an agate mortar and pestle and pressed into pellets at a pressure of 100 MPa. The pellet of the Fe compound was sealed inside an evacuated quartz ampoule to maintain the oxygen stoichiometry necessary for Fe(II). The Co and Ni compound pellets were placed inside Al_2O_3 crucibles on top of a bed of powder with the same composition in order to avoid contamination from the crucible. The sealed tube of the Fe compound was heated to 800°C, while the Co compound was annealed at 1000°C. The reactions occurred in a box furnace for two days with one intermediate grinding and repressing of the powder. The preparation of $GeNi_2O_4$ involved heating the loose powder slowly to 900°C and annealing for 12 hours, followed by grinding, pelletization, and annealing at 1100°C for 24 hours and at 1200°C for another 24 hours. Powder synchrotron x-ray diffraction was conducted at both the 11-BM beamline ($\lambda \approx 0.41317$ Å) of the Advanced Photon Source, Argonne National Laboratory and the ID31 beamline ($\lambda \approx 0.399845$ Å) of the European Synchrotron Radiation Facility. Powder coated Kapton capillaries were employed to reduce synchrotron x-ray beam heating and improve temperature equilibrium with the closed Helium cryostat exchange gas. During the study of $GeCo_2O_4$, the temperature was varied at 0.05 K/min in the temperature range $6.6\,K < T < 24\,K$, and an x-ray scan was measured every 5 minutes. The temperature difference during the course of a given scan in this temperature regime was 0.25 K. A faster temperature ramp rate of 1 K/min was applied in the temperature range $28\,K < T < 60\,K$ and a x-ray scan was measured every 2.5 min. Variable-temperature x-ray measurements of $GeNi_2O_4$ were measured at 0.5 K/min and an x-ray scan was measured every 5 minutes over the temperature range $7.5\,K < T < 130\,K$. $GeFe_2O_4$ was studied at 2 K/min, with an x-ray scan being measured every 3 minutes in the temperature range $7.7\,K < T < 130\,K$. Separate low temperature synchrotron x-ray measurements of $GeFe_2O_4$, $GeCo_2O_4$, and $GeNi_2O_4$ down to 5 K were performed at the European Synchrotron Radiation Facility. Rietveld[11] analyses were performed using GSAS/EXPGUI.[12] DICVOL, as implemented in FullProf, was used to index the low-temperature unit cell.[13] ISODISTORT was used to explore the possible crystal distortion modes and to transform the unit cell atom positions to lower symmetry.[14] Crystal structures were visualized using VESTA.[15] Magnetic properties were measured using a Quantum Design MPMS 5XL SQUID magnetometer. Capacitance was measured using a 1 V excitation in a parallel plate geometry with an Andeen-Hagerling bridge in a Quantum Design PPMS DynaCool cryostat. Prior to measurement, capacitance samples were densified through spark plasma sintering and coated with silver epoxy paste for electrodes. The processing did not affect the material crystal structure or composition, as determined by synchrotron x-ray diffraction.

III. RESULTS AND DISCUSSION

The crystal structures of powder $GeFe_2O_4$, $GeCo_2O_4$, and $GeNi_2O_4$ samples were investigated by synchrotron x-ray powder diffraction in the temperature range $6.6\,K \lesssim T \leq 295\,K$. Unit cell parameters at $T = 295\,K$ of $a_{Fe} = 8.41368(8)$ Å, $a_{Co} = 8.31910(8)$ Å, and $a_{Ni} = 8.22422(4)$ Å were extracted by Rietveld refinement of x-ray data and are in accord with prior investigations.[16–18] The known room-temperature spinel crystal structure was determined by Rietveld refinement of the diffraction pattern using the space group $Fd\bar{3}m$. A small impurity phase was detected in the $GeFe_2O_4$ sample and was determined to be 5.4 wt% of $Fe_{1.67}Ge$.[19] A $Co_{10}Ge_3O_{16}$ impurity at a level of 1.4 wt% was identified in $GeCo_2O_4$. The impurities $Fe_{1.67}Ge$ and $Co_{10}Ge_3O_{16}$, whose properties are reported by Barbier[20] and Barton *et al.*[21] respectively, have a minor influence on the results. The effects of the ferromagnetic $Fe_{1.67}Ge$ impurity on the magnetic susceptibility measurements of $GeFe_2O_4$ are discussed later in this report. Bond valence sums calculated using cation-oxygen bond parameters tabulated by Brown and Attermatt[22] are consistent with the 2+ valence state for each of these transition metal ions.[8]

Magnetic susceptibility measurements of $GeFe_2O_4$, $GeCo_2O_4$, and $GeNi_2O_4$ show that they are antiferromagnetic at low temperature. Figures 1 (a), (b), and (c) show the zero-field cooled and field cooled susceptibility measurements of $GeFe_2O_4$, $GeCo_2O_4$, and $GeNi_2O_4$ respectively. While the temperature-dependent susceptibility measurements of $GeFe_2O_4$ and $GeNi_2O_4$ are consistent with antiferromagnetic spin ordering, the susceptibility measurements of $GeFe_2O_4$ also show antiferromagnetic behavior but the susceptibility is influenced by the ferromagnetic $Fe_{1.67}Ge$ impurity. The $d\chi/dT$ curves for these spinels clearly illustrate the antiferromagnetic ordering transitions [Fig. 1(d), (e), and (f)]. The $d\chi/dT$ curve of $GeFe_2O_4$ has maxima at both $T_{N1} = 7.9\,K$ and $T_{N2} = 6.2\,K$ showing evidence for a second antiferromagnetic transition in $GeFe_2O_4$ that has not been reported [Fig. 1 (a)]. This behavior is similar to that of $GeNi_2O_4$, which is known to exhibit two transitions[10] that we observe at 11.9 K and 11.1 K [Fig. 1 (c)]. A neutron diffraction study by Matsuda *et al.* attributes

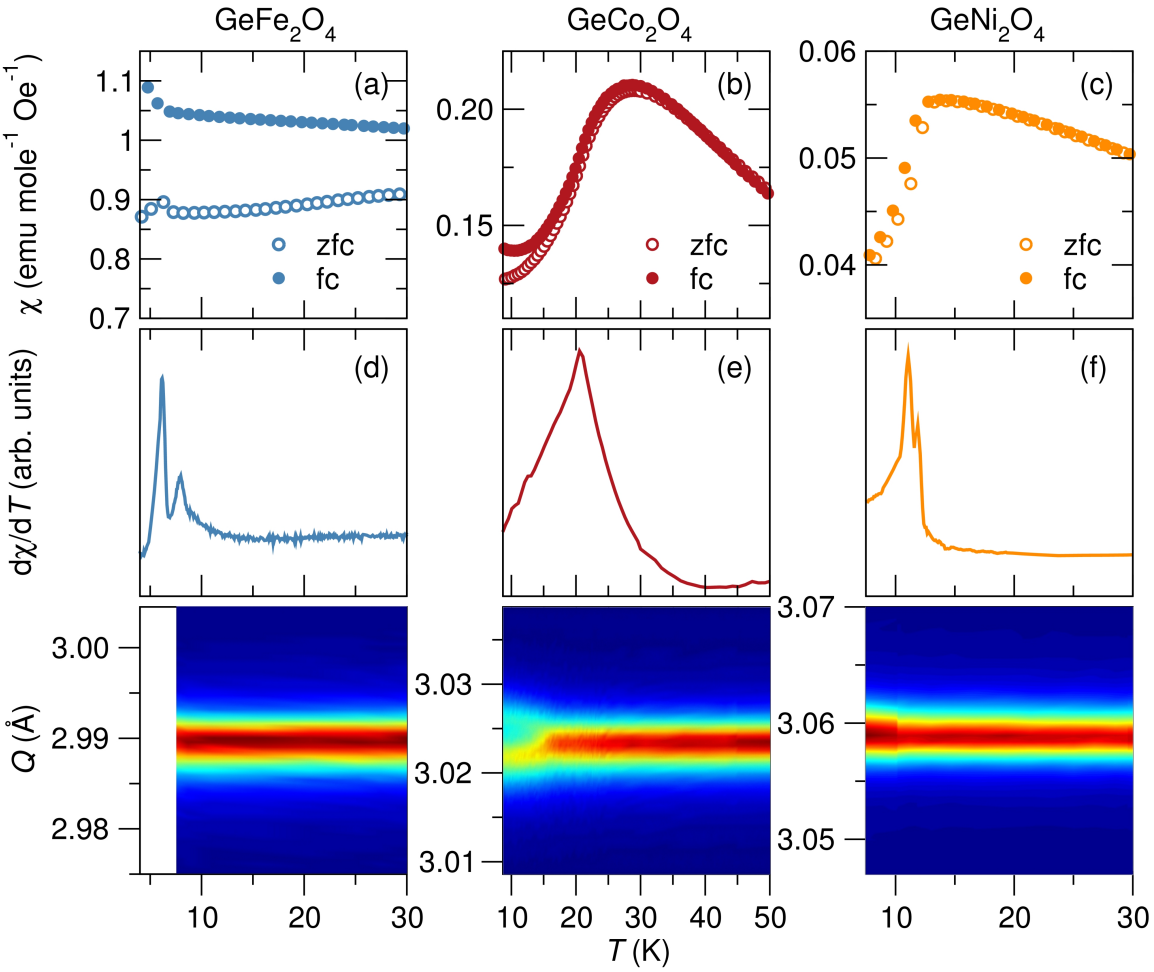

FIG. 1: (Color online) Magnetic susceptibility measurements of (a) $GeFe_2O_4$ measured in a 10 kOe field, (b) $GeCo_2O_4$ measured in a 100 Oe field, and (c) $GeNi_2O_4$ measured in a 1000 Oe field. The susceptibility measurements show antiferromagnetic ordering transitions in these GeM_2O_4 spinels. However, the magnetic susceptibility of $GeFe_2O_4$ shown in (a) is influenced by the ferromagnetic $Fe_{1.67}Ge$ impurity. The temperature-derivative of the field cooled susceptibility of (d) $GeFe_2O_4$, (e) $GeCo_2O_4$, and (f) $GeNi_2O_4$ clearly illustrate the antiferromagnetic ordering transitions of the GeM_2O_4 spinels. Two antiferromagnetic ordering transitions at 6.2 K and 7.9 K are resolved in $GeFe_2O_4$. $GeCo_2O_4$ has an antiferromagnetic transition at 20.9 K while $GeNi_2O_4$ orders antiferromagnetically at 11.1 K and 11.9 K. Variable-temperature high-resolution synchrotron x-ray powder diffraction shows no structural distortions from cubic symmetry in $GeFe_2O_4$ and $GeNi_2O_4$ (bottom panel). The cubic (400) reflections of $GeFe_2O_4$ and $GeNi_2O_4$ do not splitting in the temperature range $8\,\mathrm{K} \leq T \leq 30\,\mathrm{K}$ but a slight broadening of this reflection is observed especially in $GeNi_2O_4$ below 11 K. In contrast, the (400) cubic $Fd\bar{3}m$ reflection of $GeCo_2O_4$ splits into tetragonal $I4_1/amd$ (004) and (220) reflections at 16 K. The structural distortion of $GeCo_2O_4$ occurs below its Néel temperature of 22 K.

the two transitions of $GeNi_2O_4$ to separate orderings of the spins in the Kagome and triangular planes.[23] Curie-Weiss fitting of the high temperature susceptibility of $GeNi_2O_4$ leads to $\mu_{\mathrm{eff}} = 3.36\,\mu_{\mathrm{B}}$ and $\Theta_{\mathrm{CW}} = -11.3\,\mathrm{K}$, congruent with the literature for $GeNi_2O_4$.[24] A cusp in the $\mathrm{d}\chi/\mathrm{d}T$ of $GeCo_2O_4$ at $T_{\mathrm{N}} = 20.9\,\mathrm{K}$ indicates the onset of long-range antiferromagnetic order [Fig. 1 (b)], consistent with previous reports on $GeCo_2O_4$. Though it is not strictly valid to apply Curie-Weiss to $GeCo_2O_4$ because of Co(II) crystal field levels,[8] we find $\mu_{\mathrm{eff}} = 4.55\,\mu_{\mathrm{B}}$ and $\Theta_{\mathrm{CW}} = 55.0\,\mathrm{K}$, in reasonable agreement with the literature.[24] We are unable to analyze the magnetic susceptibility of $GeFe_2O_4$ by Curie-Weiss analysis because of the ferromagnetic $Fe_{1.67}Ge$ impurity with $T_{\mathrm{C}} = 485\,\mathrm{K}$.[25]

Variable-temperature synchrotron x-ray powder diffraction patterns show no evidence of a structural phase transition in either $GeFe_2O_4$ nor in $GeNi_2O_4$ down to $T = 8\,\mathrm{K}$ [bottom panel of Fig. 1]. A slight broadening of the cubic (400) $Fd\bar{3}m$ reflection occurs in $GeNi_2O_4$ at the Néel temperature but a splitting of the reflection is not observed. Near 8 K, $GeFe_2O_4$ and $GeNi_2O_4$ are well modeled by the cubic $Fd\bar{3}m$ structure and we determine the unit cell parameters $a_{\mathrm{Fe}} = 8.40508(1)\,\text{Å}$ and $a_{\mathrm{Ni}} = 8.21569(2)\,\text{Å}$. Separate measurements show that $GeFe_2O_4$ and $GeNi_2O_4$ retain cubic symmetry even at 5 K. The unique electronic

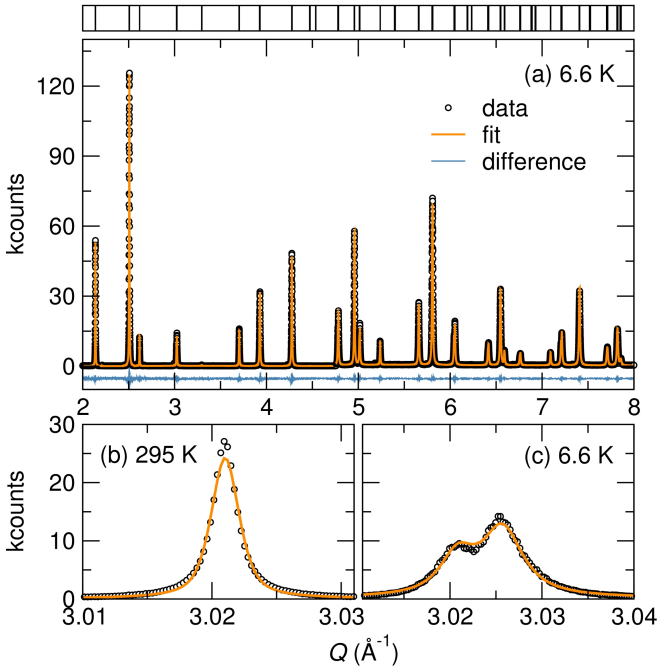

FIG. 2: (Color online) (a) Powder synchrotron x-ray diffraction of $GeCo_2O_4$ at $T = 6.6$ K modeled by Rietveld refinement to a tetragonal $I4_1/amd$ structure and 1.4 wt% $Co_{10}Ge_3O_{16}$ impurity phase. Note that data are multiplied by 5 for $Q > 4.75$ Å for visual clarity. The cubic (400) $Fd\bar{3}m$ reflection of $GeCo_2O_4$ shown in (b) splits to two tetragonal (004) and (220) reflections that are modeled by the $I4_1/amd$ structure (c).

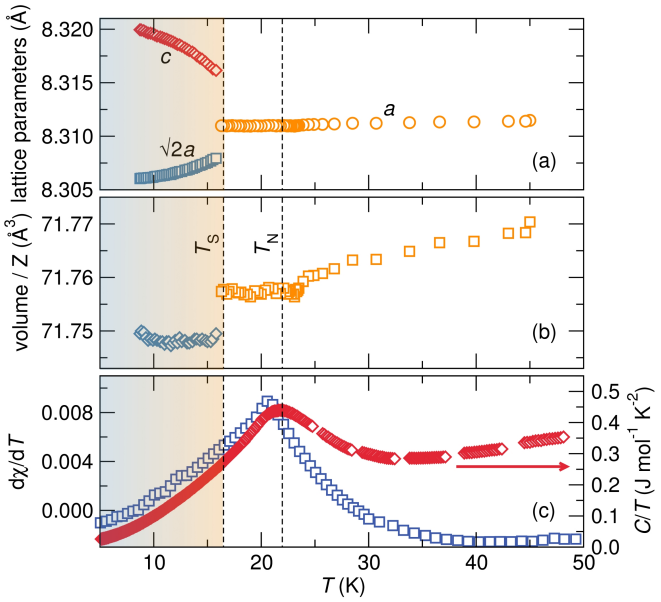

FIG. 3: (Color online) (a) At the structural distortion temperature of $GeCo_2O_4$, $T_D = 16$ K, two tetragonal lattice constants emerge from the cubic lattice constant. An elongation of the tetragonal c axis is observed. (b) The thermal evolution of the cell volume of $GeCo_2O_4$ shows two anomalies, one at the antiferromagnetic ordering temperature, $T_N = 20.9$ K, the other at the structural distortion temperature, $T_D = 16$ K. (c) $d\chi/dT$ and temperature normalized heat capacity measurements show peaks at the antiferromagnetic ordering temperature of $GeCo_2O_4$.

configuration of octahedral Ni^{2+} t_{2g}^6 e_g^2 in $GeNi_2O_4$ precludes the presence of any Jahn-Teller activity and previous studies of this material also found no evidence of a magnetostructural distortion.[26] $GeFe_2O_4$ has not been extensively studied and our measurements show no structural distortions from cubic symmetry even at 5 K, although Fe^{2+} cations are orbitally degenerate with partially filled t_{2g}^4 states. In contrast to $GeFe_2O_4$ and $GeNi_2O_4$, the (400) cubic $Fd\bar{3}m$ reflection of $GeCo_2O_4$ splits at $T_D \approx 16$ K [bottom panel of Fig. 1], confirming the onset of its known structural phase transition at low temperatures.[27] Figure 1 shows a discrepancy between the onset of antiferromagnetic order in $GeCo_2O_4$ at $T_N \approx 21$ K [Fig. 1 (b)] and the onset of the structural distortion at $T_D \approx 16$ K.

TABLE I: Structural parameters of $GeCo_2O_4$ at $T = 6.6$ K. Space group: $I4_1/amd$, $a = 5.87338(1)$ Å and $c = 8.31957(2)$ Å. The refinement figures of merit of R_{wp} and R_p are 4.34 % and 8.68 % respectively.

Site	x	y	z	U_{iso} (Å^2)
Ge	0	0.25	0.375	0.0020(1)
Co	0	0	0	0.0027(1)
O	0	0.5010(1)	0.2519(1)	0.0021(1)

We quantitatively describe the low-temperature synchrotron x-ray powder diffraction pattern of $GeCo_2O_4$ with a tetragonal $I4_1/amd$ model which is a subgroup of the $Fd\bar{3}m$ space group that is commonly used to describe other spinel systems that undergo structural distortions from cubic $Fd\bar{3}m$ symmetry.[28] The initial unit cell parameters for the tetragonal model were determined by diffraction pattern indexing and its atom positions were derived using group-subgroup theory. Figure 2 (a) displays the refinement of the $T = 6.6$ K experimental data for $GeCo_2O_4$ to the $I4_1/amd$ model. The cubic (400) reflection [Fig. 2 (b)] splits in the structurally distorted phase as shown in fig. 2 (c) and this divergence of the diffraction reflection is well described by the $I4_1/amd$ model. The small difference between the data and the structural model [Fig. 2 (a)] and refinement figures of merit [Table I] support the validity of the low-temperature tetragonal $I4_1/amd$ structural model. The extracted structural parameters for the $I4_1/amd$ tetragonal structure of $GeCo_2O_4$ at $T = 6.6$ K are listed in Table I.

We separately fit the low-temperature tetragonal $I4_1/amd$ model and the high temperature cubic $Fd\bar{3}m$ structure to the $GeCo_2O_4$ diffraction patterns in the temperature region around the transition to determine the structural phase transition temperature of $GeCo_2O_4$. Upon examining the stability of the refinements and com-

paring their figures of merit, the structural transition was determined to occur at $T_D = 16\,K$. Two tetragonal lattice constants emerge below 16 K [Fig. 3 (a)]. The tetragonal phase is characterized by $c/a > 1$ and the degree of tetragonality, increases with decreasing temperature. For both the high- and low- temperature structures, bond valence sum calculations based on Shannon-Prewitt effective ionic radii,[29] indicate the ion valences expected from the stoichiometric chemical formula, namely Ge^{4+}, Co^{2+}, and O^{2-}. The onset of the structural distortion below the Néel temperature, $T_N = 21\,K$, is unusual in comparison to our investigations of magnetostructural phase transitions in the ACr_2O_4 spinels[5,28] which show concurrent magnetic and structural transitions.

The unit cell volume of $GeCo_2O_4$ decreases with temperature, as expected for a material with a positive coefficient of thermal expansion [Fig. 3(b)]. Discontinuities in the cell volume occur at the antiferromagnetic ordering temperature, $T = 21\,K$, due to isotropic magnetostriction. Magnetostrictive effects in $GeCo_2O_4$ are consistent with large magnetostrictive and anisotropic effects that are observed in cobalt compounds because of spin-orbit coupling in high spin octahedral Co^{2+}.[30] The structural distortion of $GeCo_2O_4$ at 16 K gives rise to another discontinuity in cell volume [Fig. 3 (b)]. A change in entropy occurs at the magnetic phase transition of $GeCo_2O_4$ as illustrated by the nearly coincident anomalies in $d\chi/dT$ and the temperature normalized heat capacity [Fig. 3 (c)]. Importantly, we note that no additional magnetic or heat capacity anomalies occur at the structural transition temperature of $GeCo_2O_4$. This suggests a non-magnetic origin of this distortion. It is likely that entropy changes associated with the structural distortion at 16 K are concealed in the broad lambda-like heat capacity anomaly of $GeCo_2O_4$ that peaks at $\approx 22\,K$. The temperature normalized heat capacity shows significant entropy changes above T_N due to short range spin correlations in this temperature regime.

The temperature variation of Ge–O bond distances reveals no bond distance distortions in the cubic or tetragonal phases of $GeCo_2O_4$. As a result, in both the cubic and tetragonal phases of $GeCo_2O_4$, GeO_4 tetrahedra are described by a single bond length. CoO_6 octahedra are characterized by a single Co–O bond length in the cubic phase, however, an elongation of CoO_6 octahedra is observed in the tetragonal phase [Fig. 4 (a)]. While Jahn-Teller effects are expected to be quenched in $GeCo_2O_4$ due to strong spin-orbit coupling in Co^{2+},[31] the elongation of CoO_6 octahedra is consistent with a weak Jahn-Teller distortion that lifts orbital degeneracy by stabilizing the xz and yz orbitals of the t_{2g}^5 states. Bond distance distortions arising from the elongation of CoO_6 octahedra in the tetragonal phase are shown in Fig. 4 (b). The distortion index D is defined as $D = 1/n \sum_{i=1}^{n} (|l_i - \bar{l}|)/(\bar{l})$ where l_i is a given Co–O bond length and $\bar{l}$ is the average Co–O bond length. Figure 5 shows the cubic and tetragonal structures of $GeCo_2O_4$. The elongation of CoO_6 octahedra in the tetragonal phase yields an enhanced buckling of Co–O bonds [Fig. 5 (c) and (d)].

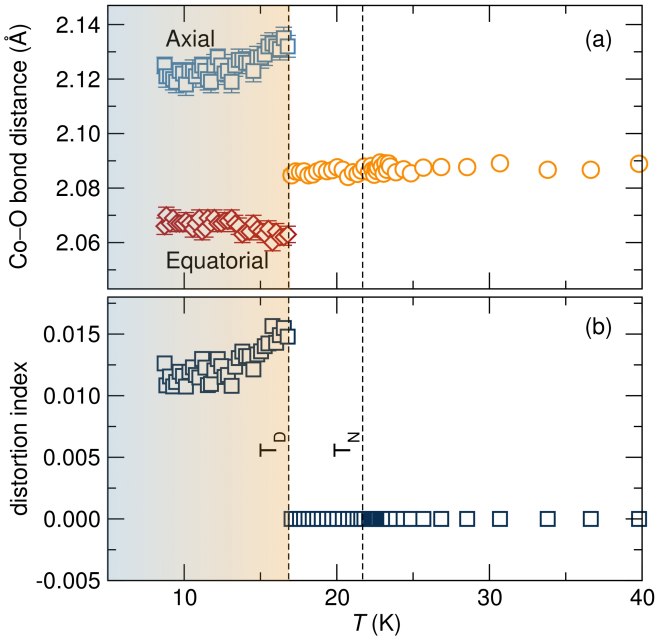

FIG. 4: (Color online) (a) While a single Co–O bond length characterizes CoO_6 octahedra in cubic $GeCo_2O_4$, two long Co–O bonds and four short Co–O bonds are observed in the tetragonal phase of $GeCo_2O_4$. (b) CoO_6 octahedra show no bond distance distortions in the cubic $Fd\bar{3}m$ phase, however, bond length distortion are observed in the tetragonal $I4_1/amd$ phase.

Concurrent with the magnetic transition of $GeCo_2O_4$ is the onset of magnetodielectric behavior. The dielectric permittivity, ϵ_r, is calculated from the capacitance measured in a parallel plate geometry by $\epsilon_r = Cd/A$. A suppression of the dielectric constant of $GeCo_2O_4$ occurs below $T_N = 21\,K$ as illustrated in Fig. 6 (a), pointing to the magnetic origin of this dielectric anomaly. The structural distortion at T_D leaves a signature in the temperature-dependent dielectric permittivity which shows a change in slope at 16 K [Fig. 6 (a)]. The lattice dielectric constant is modeled by a modified Barrett equation in the temperature range $25\,K < T < 80\,K$. The Barrett fit models the dielectric permittivity in the absence of magnetodielectric effects. The dielectric constant at $T = 2\,K$ is 0.057 % less than expected by the Barrett function, while the change in sample volume across the transition, as measured by powder synchrotron X-ray diffraction, is only 0.01 %. Thus, the change in geometry cannot be fully responsible for the observed deviation in dielectric response. Instead, this difference, whose magnitude is similar to that found in other antiferromagnetic spinels such as Mn_3O_4,[32] is likely due to a magnetodielectric effect. The frequency dependence of the dielectric properties was investigated from 1 kHz to 20 kHz, however we did not detect any significant differences in the temperature evolution or magnitude, nor did we see relaxation effects, with $\tan(\delta) < 0.0003$ for the temperatures and

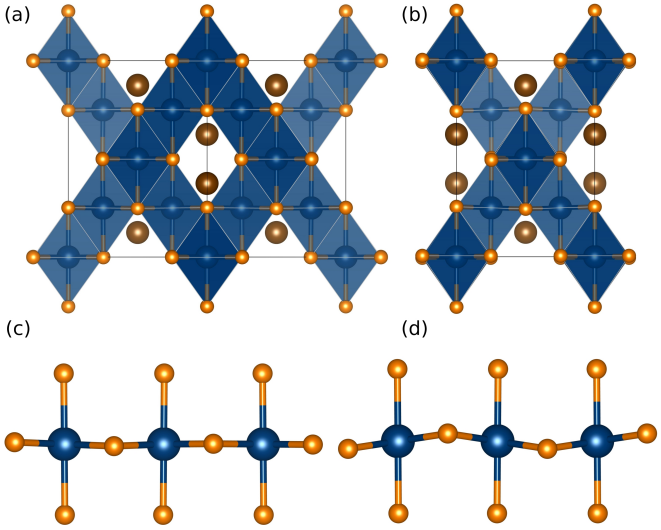

FIG. 5: (Color online) The cubic $Fd\bar{3}m$ structure of $GeCo_2O_4$ at 50 K and the low temperature tetragonal $I4_1/amd$ structure near 8 K are presented in (a) and (b) respectively. A plane of edge sharing CoO_6 octahedra in the cubic $Fd\bar{3}m$ structure (c) and in the $I4_1/amd$ structure near 8 K (d). The buckling of CoO_6 octahedra is enhanced in the tetragonal $I4_1/amd$ phase of $GeCo_2O_4$, and this likely occurs to accommodates the elongation of CoO_6 octahedra. Distortions in figures (c) and (d) have been enhanced by a factor of 5 to clearly illustrate the structural changes.

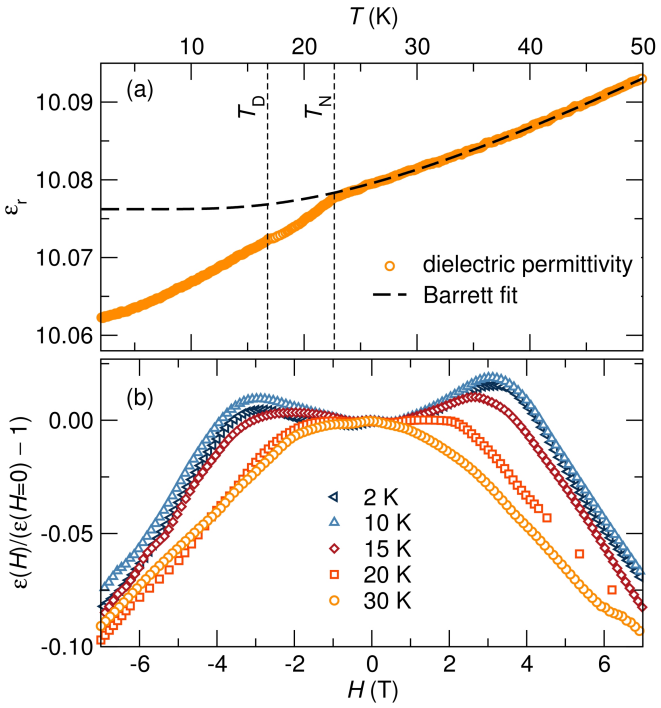

FIG. 6: (Color online) (a) The temperature dependence of the dielectric permittivity of $GeCo_2O_4$ shows a dielectric anomaly at the Néel temperature ($T_N = 21$ K). A slight change in slope of the temperature dependent dielectric constant is observed at the structural distortion temperature ($T_D = 16$ K). The Barrett fit models the dielectric permittivity well above T_N, however, the dielectric constant deviates from the Barrett function fit below T_N. (b) Relative changes in the dielectric constant of $GeCo_2O_4$ measured at 20 kHz as a function of magnetic field at different temperatures. A distinct change in the field dependence is observed beneath $T_N = 21$ K.

frequencies measured. These observations suggest that the dielectric response is not of magnetoresistive origin, and instead supports the presence of magnetodielectric coupling in $GeCo_2O_4$.[33]

The dielectric constant can be generally related to optical phonons and their frequencies by the Lyddane-Sachs-Teller relationship. It is possible to more directly connect ϵ_r to the relevant transverse-optical modes using a Barrett function, as for example, was done for $BaMnF_4$[34] and MnO,[35] and more recently for $TbFe_3(BO_3)_4$.[36] The Barrett function is $\epsilon(T) = \epsilon(0) + A/[\exp(\hbar\omega_0/k_BT)-1]$, where A is a coupling constant and ω_0 is the mean frequency of the final states in the lowest-lying optical phonon branch. The refined parameters of the fit are $\epsilon(0) = 10.0762$, $A = 0.0626$, and $\omega_0 = 339\,\mathrm{cm}^{-1}$. This ω_0, which is an average, is near the $302\,\mathrm{cm}^{-1}$ value of a transverse-optical phonon E_g mode found by Raman spectroscopy,[37] and suggests a possible spin-phonon coupling mechanism.

Further evidence that this dielectric behavior is magnetic in nature is observed in capacitance measurements performed in a varying magnetic field [Fig. 6(b)]. We plot the magnetic-field dependent dielectric permittivity with respect to the zero field permittivity using the equation $\Delta\epsilon = \epsilon(H)/\epsilon(0)-1$. As expected for a magnetodielectric, the field dependent dielectric permittivity changes below T_N. When $T > T_N$, the observed dielectric response is positive at low applied fields but becomes negative at higher fields. The transition between positive and negative responses occurs at $H = 0.5$ T for $T = 20$ K and increases to $H = 3$ T for $T = 2$ K. The magnitude of the positive upturn increases with decreasing temperature until below 10 K at which point the response begins to weaken. The asymmetry in the field-dependence in positive and negative fields is the result of magnetic hysteresis in the small $Co_{10}Ge_3O_{16}$ impurity.[21] The qualitative change in $\epsilon - H$ behavior with temperature suggests that there is substantial magnetodielectric coupling in this system. The changes in the dielectric permittivity in an applied field above T_N also occur in other antiferromagnetic magnetodielectrics and are not due to magnetodielectric effects.[32,36] Capacitance measurements revealed no magnetodielectric effects in $GeNi_2O_4$, however $GeFe_2O_4$ was not characterized.

Jahn-Teller degeneracy and spin orbit coupling in $GeCo_2O_4$

The origin of structural transitions in systems with degenerate t_{2g} states that are more than half occupied are

difficult to identify. The poor understanding of these distortions arises from the intricate interplay between spin, orbital, and lattice degrees of freedom. In understanding the structural transformation of $GeCo_2O_4$, it is illuminating to consider the related binary oxide CoO. CoO has a rocksalt crystal structure and Co^{2+} occupy octahedral sites and have the high spin $3d^7$ electronic configuration of $S = \frac{3}{2}$ and $L = 3$ observed in $GeCo_2O_4$. CoO exhibits a structural distortion at its Néel temperature, $T = 290\,K$. The origin of the structural distortion of CoO is under debate with some reports attributing it to spin-orbit coupling magnetostrictive effects[38,39] while others propose Jahn-Teller ordering.[40,41] A spin-orbit mediated structural distortion can arise from the significant spin-orbit energy $\lambda \mathbf{L} \cdot \mathbf{S}$ that is equal to or greater than the Jahn-Teller stabilization in high-spin octahedral $3d^7$ systems.[39] The structural distortion of CoO leads to a compression of CoO_6 octahedra; this distortion does not lift spin degeneracy in this material where the yz and xz orbitals remain degenerate.[40,42] However, recent high pressure experiments by Ding *et al.* have noted a decoupling of the structural and magnetic ordering in CoO under pressure; magnetic ordering occurring at higher temperatures without an accompanying lattice distortion.[41] In light of these findings, Ding *et al.* propose a Jahn-Teller mediated structural distortion in CoO which is suppressed under pressure resulting in the onset of antiferromagnetic order without an accompanying structural distortion. The same complexities in identifying the deformation mechanism in CoO are to be expected in $GeCo_2O_4$.

There are three main kinds of structural distortions in magnetic spinels. First, there are Jahn-Teller distortions that break orbital degeneracy as observed in $FeCr_2O_4$, $NiCr_2O_4$, and $CuCr_2O_4$.[28,42,43] Jahn-Teller distortions typically occur at temperatures much higher than magnetic ordering temperatures.[42] Then there are magnetostructural transformations where the onset of magnetic order changes the crystal symmetry as reported in $FeCr_2O_4$, $NiCr_2O_4$ and $CuCr_2O_4$.[28,43] It has also been shown that magnetostructural coupling is prevalent in Jahn-Teller active systems as illustrated in the spinels $FeCr_2O_4$, $NiCr_2O_4$, and $CuCr_2O_4$ by optical spectroscopy[43] and x-ray diffraction experiments.[28] When a spinel hosts more than one Jahn-Teller active cation, it undergo several structural distortions. For example, FeV_2O_4, which has Jahn-Teller V^{3+} and Fe^{2+} cations shows symmetry breaking structural distortions near 139 K, 107 K, 62 K, and 35 K due to Jahn-Teller and spin ordering.[44,45] Finally, there are spin-Jahn-Teller distortions that break the degeneracy in spin configurations, for example in $ZnCr_2O_4$ and $MgCr_2O_4$.[5,46] Like magnetostructural distortions, spin-Jahn-Teller transformations occur at the magnetic ordering temperature. Magnetostructural and spin-Jahn-Teller distortions usually involve small distortions of the lattice compared to Jahn-Teller distortions.

Previous studies of the structure and magnetism of $GeCo_2O_4$ have associated its structural distortion to magnetostrictive effects[27] that are present in octahedral Co^{2+} due to degenerate t_{2g} states.[30] The 1.001 c/a tetragonal elongation measured in $GeCo_2O_4$ below 10 K compares well with spin driven distortions in the geometrically frustrated systems $MgCr_2O_4$ and $ZnCr_2O_4$.[5] However, the onset of the distortion below the Néel temperature suggests a non-magnetic origin of this lattice distortion. A Jahn-Teller origin of this distortion is plausible given that the deformation can lift spin degeneracy by stabilizing the xz and yz orbitals of the t_{2g} states. Although the small tetragonal distortion of $GeCo_2O_4$ is at odds with large Jahn-Teller distortions observed for example in $NiCr_2O_4$,[42] a small distortion is expected in degenerate t_{2g} systems due to the weak electronic stabilization achieved through this deformation. The close proximity between the magnetic and structural ordering temperatures is in line with the competition between spin-orbit and Jahn-Teller stabilization. However, spin-orbit coupling is expected to dominate in high spin $3d^7$ complexes[31] and the precise origin of the structural deformation in $GeCo_2O_4$ should be further investigated.

The structural distortion of $GeCo_2O_4$ is not a gradual deformation that begins at the Néel temperature with a broadening of the diffraction reflections and is fully manifested below 16 K where a splitting of some of the diffraction reflections. We observe two independent structural deformations in $GeCo_2O_4$: (i) a slight structural perturbation at the Néel temperature due to magnetostrictive effects that leads to slight changes of the cubic unit cell and (ii) a structural distortion from cubic to tetragonal symmetry at 16 K which occurs independent of any magnetic ordering (bottom panel Fig. 1). While Jahn-Teller active systems such as $FeCr_2O_4$, $NiCr_2O_4$ and $CuCr_2O_4$ show symmetry breaking structural transitions at both the orbital and spin ordering transition temperature, $GeCo_2O_4$ shows different behavior where spin ordering yields a mere change of its cubic lattice constant while a structural distortion independent of magnetism occurs below its Néel temperature.

IV. CONCLUSIONS

A structural phase transition was observed in the spinel $GeCo_2O_4$ at $T_D = 16\,K$ using variable-temperature high-resolution synchrotron powder x-ray diffraction and physical property measurements. An analogous transition was not observed in $GeFe_2O_4$ or $GeNi_2O_4$. Unlike many other magnetic spinels, the magnetic and structural transitions of $GeCo_2O_4$ are not coincident and we discuss the decoupling of structural and magnetic ordering in this system considering the effects of magnetostriction and Jahn-Teller ordering. We report the first complete description of the low-temperature $I4_1/amd$ crystal structure of $GeCo_2O_4$ with $c/a > 1$. In $GeFe_2O_4$, we observe a second antiferromagnetic transition, not previously reported, that is reminiscent of $GeNi_2O_4$ because it is close in proximity to another transition

slightly higher in temperature. Finally, we present evidence for magnetodielectric coupling in $GeCo_2O_4$ beneath T_N.

V. ACKNOWLEDGMENTS

We thank Professor Gavin Lawes for preliminary measurements on $GeCo_2O_4$ and Dr. John Mitchell for helpful discussions. We thank Dr. Christina Birkel for SPS. This project was supported by the NSF through the DMR 1105301. PTB is supported by the NSF Graduate Research Fellowship Program. MCK is supported by the Schlumberger Foundation Faculty for the Future fellowship. MWG is supported by a NSERC Postgraduate Scholarship and an International Fulbright Science & Technology Award. We acknowledge the use of MRL Central Facilities which are supported by the MRSEC Program of the NSF under Award No. DMR 1121053; a member of the NSF-funded Materials Research Facilities Network (www.mrfn.org). Use of data from the 11-BM beamline at the Advanced Photon Source was supported by the U.S. Department of Energy, Office of Science, Office of Basic Energy Sciences, under Contract No. DE-AC02-06CH11357. Data were also collected on the ID31 beamline at the European Synchrotron Radiation Facility (ESRF), Grenoble, France. We thank Andy Fitch and Caroline Curfs for providing assistance in using beamline ID31.

* Electronic address: kemei@mrl.ucsb.edu
† Electronic address: seshadri@mrl.ucsb.edu

[1] S. Kondo, D. C. Johnston, C. A. Swenson, F. Borsa, A. V. Mahajan, L. L. Miller, T. Gu, A. I. Goldman, M. B. Maple, D. A. Gajewski, et al., Phys. Rev. Lett. **78**, 3729 (1997).
[2] Y. Yamasaki, S. Miyasaka, Y. Kaneko, J.-P. He, T. Arima, and Y. Tokura, Phys. Rev. Lett. **96**, 207204 (2006).
[3] S. Bordacs, D. Varjas, I. Kezsmarki, G. Mihaly, L. Baldassarre, A. Abouelsayed, C. A. Kuntscher, K. Ohgushi, and Y. Tokura, Phys. Rev. Lett. **103**, 077205 (2009).
[4] A. D. LaForge, S. H. Pulido, R. J. Cava, B. C. Chan, and A. P. Ramirez, Phys. Rev. Lett. **110**, 017203 (2013).
[5] M. C. Kemei, P. T. Barton, S. L. Moffitt, M. W. Gaultois, J. A. Kurzman, R. Seshadri, M. R. Suchomel, and Y.-I. Kim, J. Phys.: Condens. Matter **25**, 326001 (2013).
[6] G. Blasse and J. F. Fast, Philips Res. Rep. **18**, 393 (1963).
[7] E. W. Gorter, J. Appl. Phys **34**, 1253 (1963).
[8] J. C. Lashley, R. Stevens, M. K. Crawford, J. Boerio-Goates, B. F. Woodfield, Y. Qiu, J. W. Lynn, P. A. Goddard, and R. A. Fisher, Phys. Rev. B **78**, 104406 (2008).
[9] S. Diaz, S. de Brion, G. Chouteau, B. Canals, V. Simonet, and P. Strobel, Phys. Rev. B **74**, 092404 (2006).
[10] M. K. Crawford, R. L. Harlow, P. L. Lee, Y. Zhang, J. Hormadaly, R. Flippen, Q. Huang, J. W. Lynn, R. Stevens, B. F. Woodfield, et al., Phys. Rev. B **68**, 220408 (2003).
[11] H. M. Rietveld, J. Appl. Crystallogr. **2**, 65 (1969).
[12] B. H. Toby, J. Appl. Crystallogr. **34**, 210 (2001).
[13] A. Boultif and D. Louer, J. Appl. Crystallogr. **37**, 724 (2004).
[14] B. J. Campbell, H. T. Stokes, D. E. Tanner, and D. M. Hatch, J. Appl. Crystallogr. **39**, 607 (2006).
[15] K. Momma and F. Izumi, J. Appl. Crystallogr. **41**, 653 (2008).
[16] M. D. Welch, M. A. Cooper, and F. C. Hawthorne, Mineral. Mag. **65**, 441 (2001).
[17] H. Furuhashi, M. Inagaki, and S. Naka, J. Inorg. Nucl. Chem. **35**, 3009 (1973).
[18] K. Hirota, T. Inoue, N. Mochida, and A. Ohtsuka, J. Ceram. Soc. Jpn. **98**, 976 (1990).
[19] K. Kanematsu and T. Ohoyama, J. Phys. Soc. Jpn. **20**, 236 (1965).
[20] J. Barbier, Acta Crystallogr. C **51**, 343 (1995).
[21] P. T. Barton, R. Seshadri, A. Llobet, and M. R. Suchomel, Phys. Rev. B **88**, 024403 (2013).
[22] I. D. Brown and D. Altermatt, Acta Crystallogr. B **B41**, 244 (1985).
[23] M. Matsuda, J.-H. Chung, S. Park, T. J. Sato, K. Matsuno, H. A. Katori, H. Takagi, K. Kakurai, K. Kamazawa, Y. Tsunoda, et al., Europhys. Lett. **82**, 37006 (2008).
[24] S. Diaz, S. de Brion, M. Holzapfel, G. Chouteau, and P. Strobel, Physica B **346**, 146 (2004).
[25] K. Yasukōchi, T. Ohoyama, and K. Kanematsu, J. Phys. Soc. Jpn. **16**, 429 (1961).
[26] M. K. Crawford, R. L. Harlow, P. L. Lee, Y. Zhang, J. Hormadaly, R. Flippen, Q. Huang, J. W. Lynn, R. Stevens, B. F. Woodfield, et al., Phys. Rev. B(R) **68**, 220408 (2003).
[27] T. Hoshi, H. A. Katori, M. Kosaka, and H. Takagi, J. Magn. Magn. Mater. **310**, e448 (2007).
[28] M. R. Suchomel, D. P. Shoemaker, L. Ribaud, M. C. Kemei, and R. Seshadri, Phys. Rev. B **86**, 054406 (2012).
[29] R. D. Shannon and C. T. Prewitt, Acta Crystallogr. B **25**, 925 (1969).
[30] J. C. Slonczewski, J. Appl. Phys. **32**, 253S (1961).
[31] J. Kanamori, Prog. Theor. Phys. **17**, 197 (1957).
[32] R. Tackett, G. Lawes, B. C. Melot, M. Grossman, E. S. Toberer, and R. Seshadri, Phys. Rev. B **76**, 024409 (2007).
[33] G. Catalan, Appl. Phys. Lett. **88**, 102902 (2006).
[34] D. L. Fox, D. R. Tilley, J. F. Scott, and H. J. Guggenheim, Phys. Rev. B **21**, 2926 (1980).
[35] M. S. Seehra and R. E. Helmick, Phys. Rev. B **24**, 5098 (1981).
[36] U. Adem, L. Wang, D. Fausti, W. Schottenhamel, P. H. M. van Loosdrecht, A. Vasiliev, L. N. Bezmaternykh, B. Büchner, C. Hess, and R. Klingeler, Phys. Rev. B **82**, 064406 (2010).
[37] J. A. Koningstein, J. M. Preudhomme, P. A. Grunberg, and J. T. Hoff, J. Chem. Phys. **56**, 354 (1972).
[38] W. Jauch, M. Reehuis, H. J. Bleif, F. Kubanek, and P. Pattison, Phys. Rev. B **64**, 052102 (2001).
[39] J. B. Goodenough, Magnetism and the chemical bond (John Wiley and Sons, New York-London) **1**, 213 (1963).
[40] W. Jauch and M. Reehuis, Phys. Rev. B **65**, 125111 (2002).
[41] Y. Ding, Y. Ren, P. Chow, J. Zhang, S. C. Vogel, B. Winkler, J. Xu, Y. Zhao, and H.-K. Mao, Phys. Rev. B **74**, 144101 (2006).
[42] J. D. Dunitz and L. E. Orgel, J. Phys. Chem. Solids **3**, 20

(1957).
[43] V. Kocsis, S. Bordacs, D. Varjas, K. Penc, A. Abouelsayed, C. A. Kuntscher, K. Ohgushi, Y. Tokura, and I. Kezsmarki, Phys. Rev. B **87**, 064416 (2013).
[44] S. Kawaguchi, H. Ishibashi, S. Nishihara, M. Miyagawa, K. Inoue, S. Mori, and Y. Kubota, J. Phys.: Condens. Matter **25**, 416005 (2013).
[45] T. Katsufuji, T. Suzuki, H. Takei, M. Shingu, K. Kato, K. Osaka, M. Takata, H. Sagayama, and T. Arima, J. Phys. Soc. Jpn. **77**, 053708 (2008).
[46] S. E. Dutton, Q. Huang, O. Tchernyshyov, C. L. Broholm, and R. J. Cava, Phys. Rev. B **83**, 064407 (2011).